Applications of Fractional Lower Order Time-frequency Representation to Machine Bearing Fault Diagnosis

Junbo Long, Haibin Wang, Peng Li, and Hongshe Fan

***Abstract*—The machinery fault signal is a typical non-Gaussian and non-stationary process. The fault signal can be described by $S\alpha S$ distribution model because of the presence of impulses. Time-frequency distribution is a useful tool to extract helpful information of the machinery fault signal. Various fractional lower order (FLO) time-frequency distribution methods have been proposed based on fractional lower order statistics, which include fractional lower order short time Fourier transform (FLO-STFT), fractional lower order Wigner-Ville distributions (FLO-WVDs), fractional lower order Cohen class time-frequency distributions (FLO-CDs), fractional lower order adaptive kernel time-frequency distributions (FLO-AKDs) and adaptive fractional lower order time-frequency auto-regressive moving average (FLO-TFARMA) model time-frequency representation method. The methods and the exiting methods based on second order statistics in $S\alpha S$ distribution environments are compared, simulation results show that the new methods have better performances than the existing methods. The advantages and disadvantages of the improved time-frequency methods have been summarized. Last, the new methods are applied to analyze the outer race fault signals, the results illustrate their good performances.**

***Index Terms*—adaptive function, Alpha stable distribution, auto-regressive (AR) model, non-stationary signal, parameter estimation, time frequency representation.**

I. Introduction

THE machinery vibration signal is a non-stationary signal, its spectrum characteristic changes with the time. The time-frequency analysis is a powerful tool to provide the frequency spectrum information for the non-stationary signals. The traditional short time Fourier transform (STFT) time-frequency distributions [1], Wigner-Ville distributions (WVDs) [2], wavelet transform (WT) time-frequency [3], Hilbert-Huang transform (HHT) time-frequency [4]−[6], the time-frequency analysis methods have been widely used in mechanical fault diagnosis. Recently, some improved methods based on traditional time-frequency distribution are also used in fault diagnosis, such as the evolutionary spectrum based on STFT [6] and the improved cyclic WVD spectrum analysis based on WVD [7]. The time-frequency distribution cannot change according to the signal's characteristic, hence, the adaptive time-frequency analysis method has been focused and applied to the mechanical fault diagnosis because of its high performance. The time-frequency analysis method based on adaptive kernel function is proposed in [8], and the adaptive optimization criterion can adaptively adjust the kernel function according to the characteristics of the signals.

Recently, the adaptive time-frequency analysis method is developed rapidly, such as adaptive time-frequency distribution based on radial Gaussian kernel function, cone-shaped kernel function [9], [10] and butterworth kernel function [11]. The new adaptive parabola kernel function time-frequency distribution method has been proposed in [12]. The improved basis function chirplet adaptive time-frequency method is introduced in [13], and it is applied to the bearings and gear box fault analysis. An improved radial parabolic kernel time-frequency method has been used to the bearing fault diagnosis, which can effectively improve the bearing fault diagnosis time-frequency resolution and suppress the cross-term interference [14]. Shi *et al.* proposed a kind of adaptive time-frequency decomposition algorithm based on Gaussian linear frequency-modulation [15], the method has good performance in the machinery critical vibration analysis. Recently, the adaptive time-frequency method is proposed based on AR parameter model by Jachan *et al.* [16], [17], whereafter, the improved vector time-frequency AR (VTFAR) and TFARMA adaptive time-frequency algorithm are put forward [18], [19]. The model time-frequency methods have been applied in mechanical engineering [20], [21], the TFAR model method has illustrated fine time-frequency resolution when it is used to analyze the vibration signals of a faulty gearbox [20], more application examples with parametric models method could be found in [21]. However, the TFARMA model method has not been applied for the machinery fault signals analysis.

Gaussian model and second order statistics are used to analyze the fault signals in the above methods, but some actual mechanical fault signals have obvious pulsing characteristics, and they are non-Gaussian, hence there will be a certain deviation. Therefore, Nikias first proposed a new statistical

Manuscript received September 25, 2015, accepted February 18, 2016. This work was supported by the National Natural Science Foundation of China (61261046, 61362038), the Natural Science Foundation of Jiangxi Province (20142BAB207006, 20151BAB207013), the Science and Technology Project of Provincial Education Department of Jiangxi Province (GJJ14738, GJJ14739), the Research Foundation of Health Department of Jiangxi Province (20175561), and the Science and Technology Project of Jiujiang University (2016KJ001, 2016KJ002). Recommended by Associate Editor YangQuan Chen. *(Corresponding author: Junbo Long.)*

Citation: J. B. Long, H. B. Wang, P. Li, and H. S. Fan, "Applications of fractional lower order time-frequency representation to machine bearing fault diagnosis," *IEEE/CAA J. of Autom. Sinica*, vol. 4, no. 4, pp. 734−750, Oct. 2017.

J. B. Long, H. B. Wang, P. Li, and H. S. Fan are with the Department of Electrical and Engineering, Jiujiang University, Jiujiang 332005, China (e-mail: ljb829@qq.com; wanghaibin00@163.com; jjxylipeng@126.com; fanhongshe@126.com).

Color versions of one or more of the figures in this paper are available online at http://ieeexplore.ieee.org.

Digital Object Identifier 10.1109/JAS.2016.7510190

model for the typical signal Alpha (α) stable distribution process [22]−[25]. When $0 < \alpha < 2$, the performance of the time-frequency analysis method based on Gaussian model degenerates, therefore, the new methods based on α stable distribution model are put forward, and they are applied to the mechanical fault diagnosis. Li *et al.* proved that the bearing fault signals belong to α stable distribution [26]. A new support vector machine fault diagnosis algorithm based on the stable distribution model is proposed in [27], it can effectively improve small sample learning and convergence speed. A rolling bearing fault diagnosis method is put forward with fractional lower order statistics instead of second order statistics based on α stable model and kurtogram [28], which effectively improve the performance. However, few research works are studied on applications of time-frequency distribution in machine fault diagnosis with α stable distribution model. The adaptive time-frequency analysis method based on α stable distribution is worth investigating. More realistic statistical model will bring new machine fault detection and diagnosis methods for rotating machines. In addition, the fractional-order differential calculus methods have been applied in many fields [29]−[31].

In this paper, several new time-frequency representation methods based on α stable distribution statistical modeling are proposed for machine fault diagnosis. The paper is structured in the following manner. α stable distribution and its statistical moment are introduced in Section II. The bearing fault signals are introduced in Section III. The improved fractional lower order time-frequency representation methods are demonstrated, and the simulations comparisons with the conventional methods are performed to demonstrate justifiability of the proposed methods in Section IV. The simulations of the outer race fault signals diagnosis are presented in Section V. Finally, the conclusions and future research are given in Section VI.

II. α Stable Distribution and Its Statistics

A. α Stable Distribution

α stable distribution is a kind of generalized Gaussian distribution, the process is not limited in variance and its probability density function has a serious tail, its characteristic function can be described as [22]−[25]

$$\phi(t) = \exp\{j\mu t - \gamma|t|^{\alpha}[1 + j\beta \text{sign}(t)\omega(\tau, \alpha)]\} \quad (1)$$

where α is the characteristic index, when $0 < \alpha < 2$ it (type 1) is lower order α stable distribution, when $\alpha = 2$ it is Gaussian distribution. β is the symmetry coefficient, γ is the dispersion coefficient, μ is the location parameter. When $\beta = 0$, $\mu = 0$, $\gamma = 1$, When $\alpha = 0.5$, 1.0, 1.5, and 2.0, the time-domain waveforms of $S\alpha S$ distribution are shown in Fig. 1, and their probability density function (PDF) are shown in Fig. 2.

Waveforms of $S\alpha S$ stable dαvariance are shown in Fig. 3 when sample numbers successively increase with $\alpha = 0.5$, 1.0, 1.5, and 2.0. When $0 < \alpha < 2$, the results show that vari-

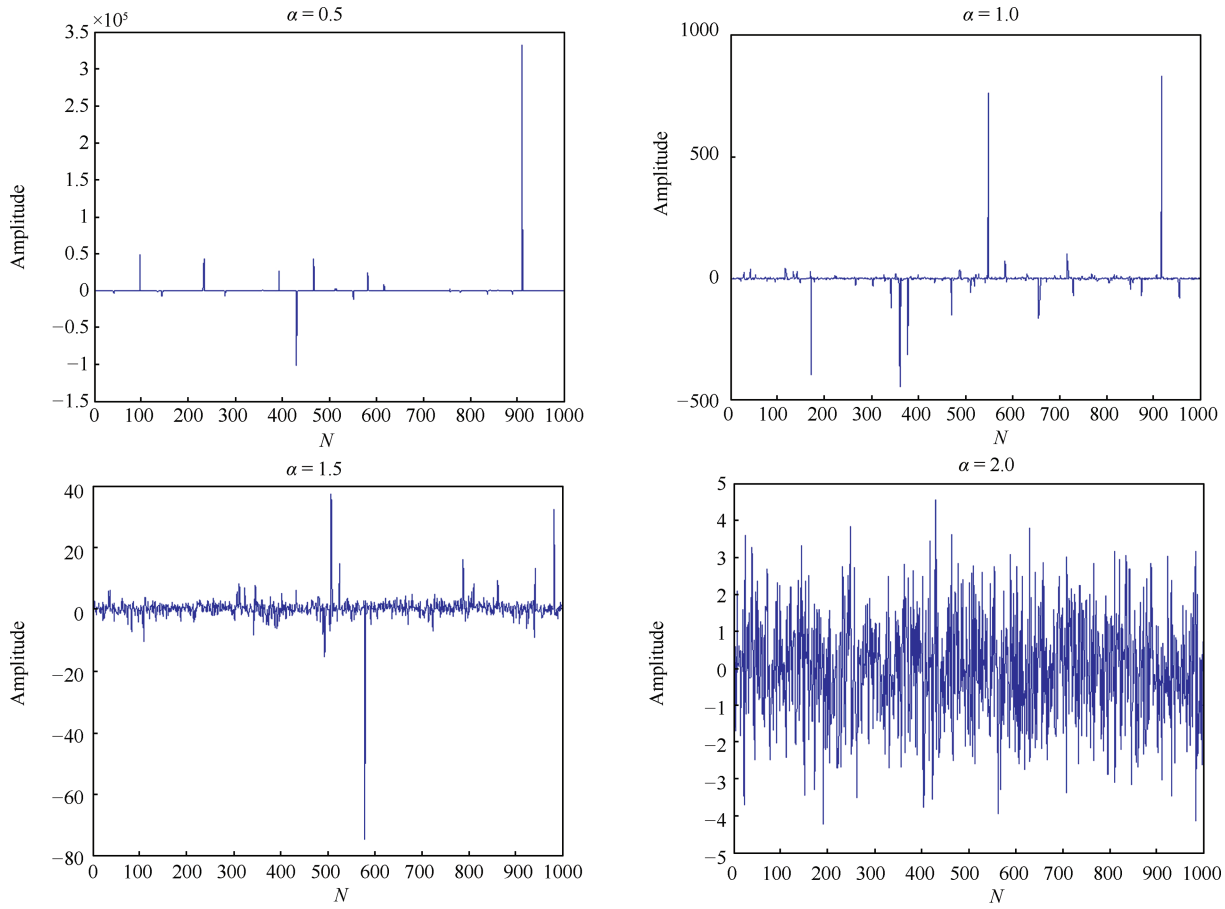

Fig. 1. Waveform of $S\alpha S$ distribution under $\alpha = 0.5$, 1.0, 1.5, and 2.0 in time domain.

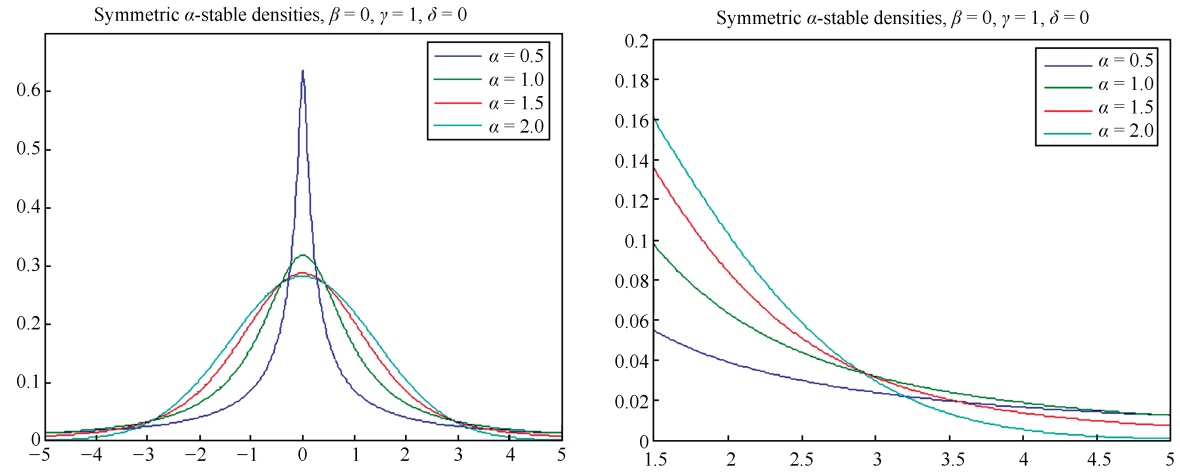

Fig. 2. PDF of $S\alpha S$ distribution with different alpha (α).

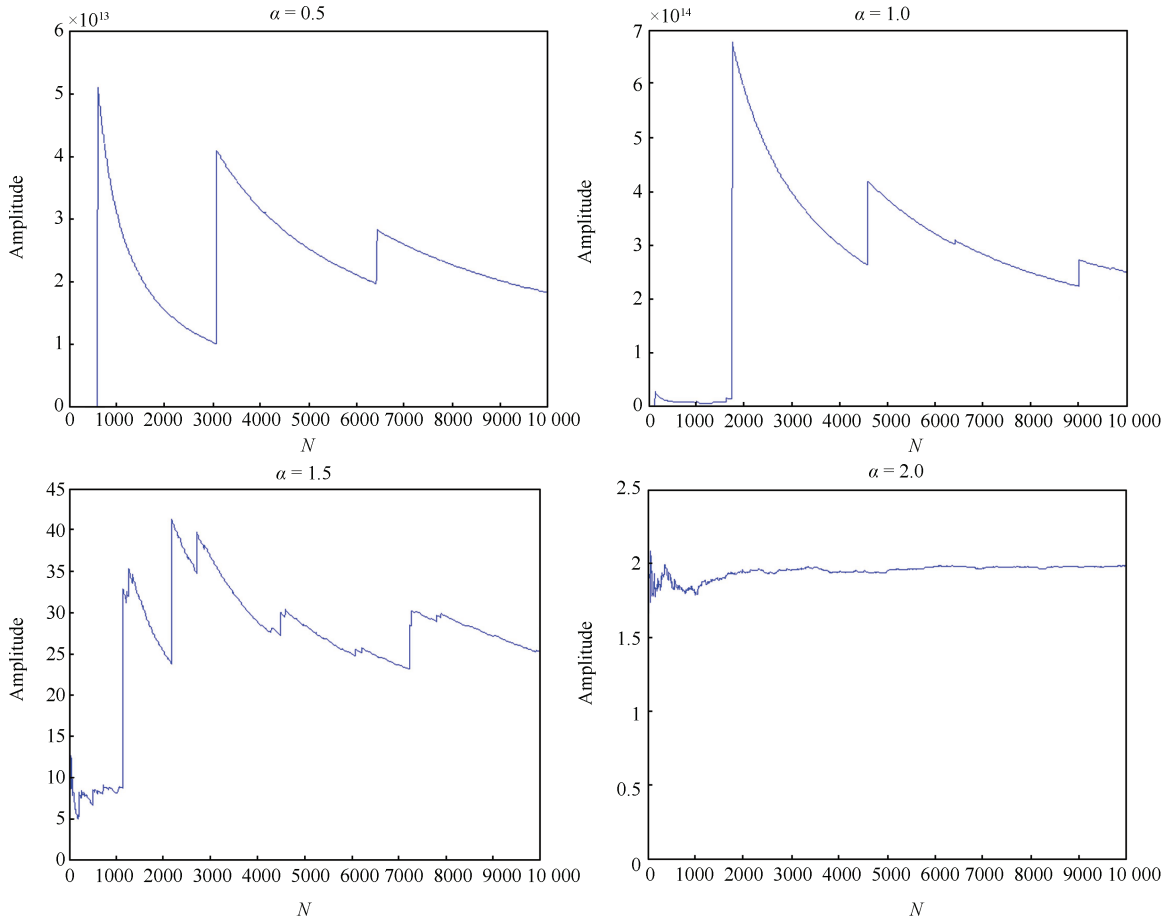

Fig. 3. Variance of $S\alpha S$ distribution with successively increase of sample numbers with different alpha (α).

ances are not limited, the variance is convergent when $\alpha = 2$ (Gaussian distribution), $\gamma = 2\sigma^2 = 2$ ($\sigma = 1$).

B. Fractional Lower Order Statistics

1) Fractional Lower Order Covariation Coefficient: The covariance of $S\alpha S$ distribution is not existing because of its limited variance. Hence, the covariation concept is put forward by Miller in 1978, it is similar to the covariance of Gaussian random process. Covariation of two $S\alpha S$ distribution random variables X and Y is defined as

$$[X, Y]_\alpha = \int_s xy^{\langle \alpha-1 \rangle} \mu ds, \quad 1 < \alpha \leq 2 \tag{2}$$

where S denotes the unit circle, $\langle \cdot \rangle$ denotes the operation $z^{\langle \alpha \rangle} = |z|^\alpha \text{sign}(z)$, the covariation coefficient of $X$and Y is defined as

$$\lambda_{XY} = \frac{[X, Y]_\alpha}{[Y, Y]_\alpha}. \tag{3}$$

If the dispersion coefficient of Y is γ_y, the covariation and covariation coefficient can be written as

$$[X,Y]_\alpha = \frac{E(XY^{\langle p-1\rangle})}{E(|Y|^p)}\gamma_y, \quad 1 \le p < \alpha \le 2 \tag{4}$$

$$\lambda_{XY} = \frac{E(XY^{\langle p-1\rangle})}{E(|Y|^p)}, \qquad 1 \le p < \alpha \le 2. \tag{5}$$

According to the definition of covariation coefficient, the covariation coefficient of a real observation sequence $X(n)$ $(n = 0, 1, \ldots, N)$ can be defined as [21]:

$$\lambda(m) = \frac{E(X(n)X(n+m)^{\langle p-1\rangle})}{E(|X(n+m)|^p)}, \quad 1 \le p < \alpha \le 2 \tag{6}$$

$$\hat{\lambda}(m) = \frac{\sum_{m=1}^{N} X(n)|X(n+m)|^{p-1}\text{sign}[X(n+m)]}{\sum_{m=1}^{N} |X(n+m)|^p}, \quad 1 \le p < \alpha \le 2 \tag{7}$$

where $\hat{\lambda}(m)$ is the approximate estimation of $\lambda(m)$. The simplified fractional lower order moment is used in array signal processing, and it is expressed as [23], [24]:

$$\lambda_{\text{FLOM}}(m) = E(X(n)X(n+m)^{\langle p-1\rangle}), \quad 1 \le p < \alpha \le 2 \tag{8}$$

when $X(n)$ is real

$$\hat{\lambda}_{\text{FLOM}}(m) = \frac{1}{L_2 - L_1}\sum_{n=L_1+1}^{L_2} X(n)|X(n+m)|^{p-1}\text{sign}[X(n+m)] \tag{9}$$

when $X(n)$ is complex

$$\hat{\lambda}_{\text{FLOM}}(m) = \frac{1}{L_2 - L_1}\sum_{n=L_1+1}^{L_2} X(n)|X(n+m)|^{p-2}X^*(n+m) \tag{10}$$

where $1 \le p < \alpha \le 2$, $L_1 = \max(0, -m)$, $L_2 = \min(N - m, N)$.

2) Fractional Lower Order Covariance: Because the fractional lower order covariation and fractional lower order moment define α as $1 < \alpha \le 2$ and the range from 0 to 1 is not defined, hence, fractional lower order covariance (FLOC) is given in [25], in which $0 < \alpha \le 2$ is defined. Fractional lower order auto-covariance (FLOAC) of N pairs of the observations $X(n)$ $(n = 0, 1, \ldots, N)$ based on the definition of FLOC [25] can be defined as:

$$R_d(m) = E\left\{X(n)^{\langle a\rangle}X(n+m)^{\langle b\rangle}\right\}, \quad 0 \le a < \frac{\alpha}{2}, \ \ 0 \le b < \frac{\alpha}{2} \tag{11}$$

where $0 < \alpha \le 2$, if $X(n)$ is real, the FLOAC can be estimated with the sample FLOAC $\hat{R}_d(m)$.

$$\hat{R}_d(m) = \frac{1}{L_2 - L_1} \times \sum_{n=L_1+1}^{L_2} |X(n)|^a|X(n+m)|^b\text{sign}[X(n)X(n+m)] \tag{12}$$

and if $X(n)$ is complex, the FLOAC is estimated with the sample FLOAC $\hat{R}_d(m)$

$$\hat{R}_d(m) = \frac{1}{L_2 - L_1} \times \sum_{n=L_1+1}^{L_2} |X(n)|^{a-1}|X(n+m)|^{b-1}X^*(n)X^*(n+m) \tag{13}$$

where $L_1 = \max(0, -m)$, $L_2 = \min(N-m, N)$, "$*$" denotes the conjugate operation.

III. Bearing Fault Signals

The data of real bearing fault signals are got from the Case Western Reserve University (CWRU) bearing data center [32]. As shown in Fig. 4, the diameter of the bearing fault in the test motor is 0.007 inches, and the fault points include inner race fault, ball fault and outer race fault. The experiments are conducted with a 2 hp reliance electric motor, and the acceleration data are measured at proximal and distal points of motor bearings, the points include the drive end accelerometer (DE), fan end accelerometer (FE) and base accelerometer (BA). The motor speed is 1797 RPM (revolutions per minute), and the digital data are collected with a speed of 12 000 samples per second.

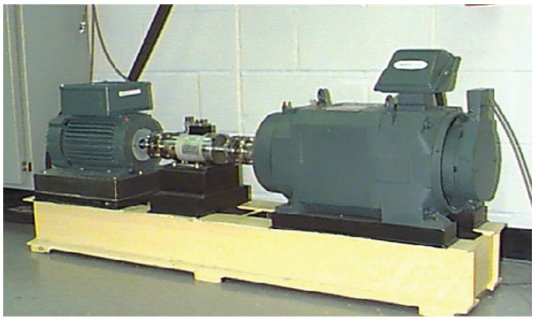

Fig. 4. The apparatus of bearing fault test data.

When the single fault point appears in inner race, outer race or ball, we collect the fault signals. Waveforms are shown in Figs. 5 (a)−5 (d), where it is shown that fault points cause different impulse intensities. The ball fault has very small impulse intensity, while the impulse intensity of outer race is higher.

Statistical characteristics of these bearing fault signals should be analyzed to obtain the condition information. Hence, the stable distribution statistical model is used to estimate parameters of the inner race fault signals, ball fault signals and outer race fault signals, the estimated four parameters are shown in Table I. As it can be seen, bearing signals in normal condition are Gaussian distribution for $\alpha = 2$, and they are non-Gaussian α stable distribution for $\alpha < 2$. Probability density function (PDF) of the inner race fault signals, the ball fault signals and the outer race fault signals are shown in Fig. 6. By comparing PDF of normal signals and fault signals, we know that PDF of fault signals have serious trailing. Table I shows that the β value around zero, and Fig. 6 shows that bearing fault signals generally have symmetric PDF, hence,

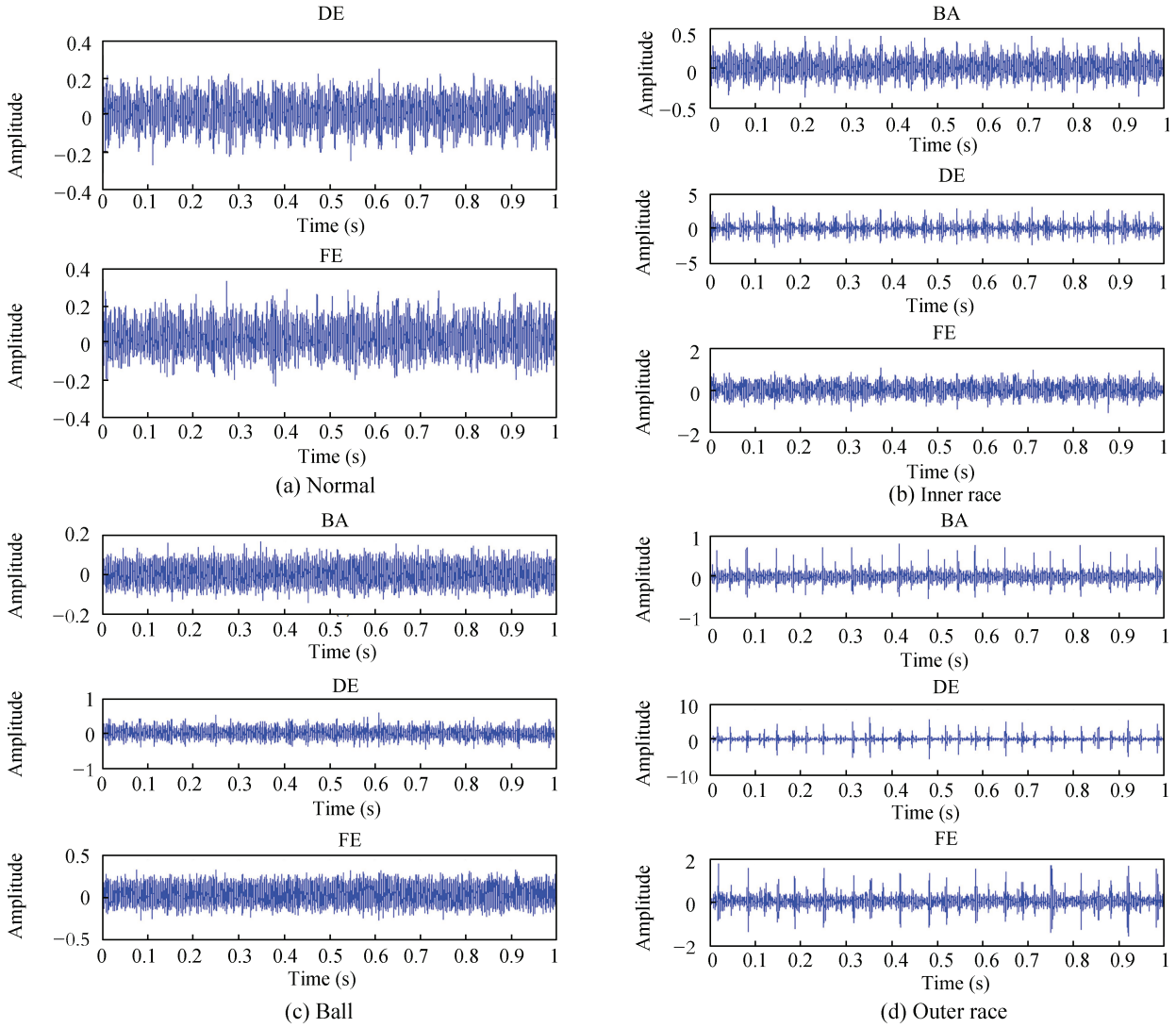

Fig. 5. Bearing fault waveforms. (a) The waveform of normal signals in DE and FE. (b) The waveform of the inner race fault signals in DE, FE and BA. (c) The waveform of the ball fault signals in DE, FE and BA. (d) The waveform of the outer race fault signals in DE, FE and BA.

$S\alpha S$ distribution statistical model is concise and accurate for bearing fault signals.

TABLE I
α STABLE DISTRIBUTION MODEL PARAMETER ESTIMATES OF BEARING FAULT SIGNALS

Parameters		α	β	γ	μ
Normal	DE	2.000	–0.283	0.1304	0.1317
	FE	2.000	1.000	0.0583	0.0236
Inner race	BA	1.7682	0.0872	0.0590	0.0062
	DE	1.4195	0.0155	0.2407	0.0175
	FE	1.8350	0.0322	0.1495	0.0291
Ball	BA	1.9790	0.0592	0.0293	0.0055
	DE	1.8697	0.1215	0.0772	0.0193
	FE	1.998	–0.0371	0.0674	0.0321
Outer race	BA	1.6077	–0.1731	0.0530	0.0012
	DE	1.1096	0.0433	0.1341	0.0367
	FE	1.5435	–0.0169	0.0968	0.0296

IV. FRACTIONAL LOWER ORDER TIME-FREQUENCY DISTRIBUTIONS

A. Fractional Lower Order Short-time Fourier Transform

1) Principle: Short time Fourier transform (STFT) time-frequency distribution is free from cross-term interference, but the time-frequency resolution is low and it is governed by the Heisenberg uncertainty principle. The conventional STFT of an analytic signal $x(t)$ is defined as

$$STFT_x(t,\omega)=\int_{-\infty}^{+\infty}x(\tau)h(\tau-t)e^{-j\omega\tau}d\tau. \tag{14}$$

The discrete equation is defined as

$$STFT_x(n,\varpi)=\sum_m x(m)h(m-n)e^{-jn\varpi}. \tag{15}$$

STFT is one of Fourier transform, which is added with time window $h(t)$ at each specific time of $x(t)$, in α stable distribution environment, fractional low order short time Fourier transform (FLO-STFT) based on P order moment can be defined as

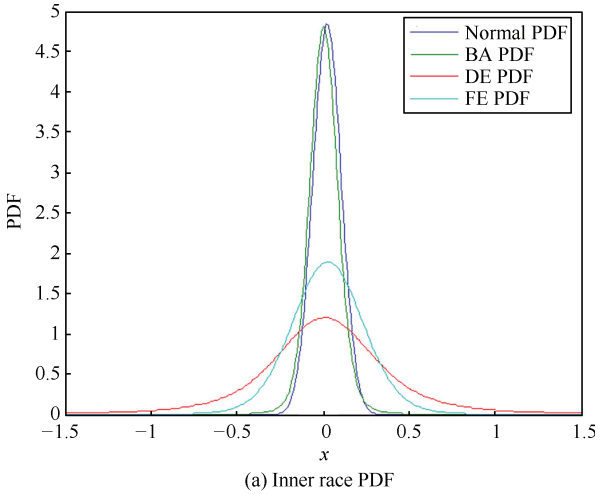

(a) Inner race PDF

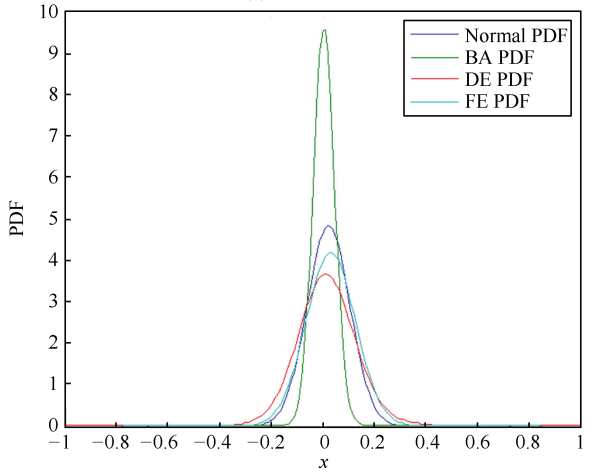

(b) Ball PDF

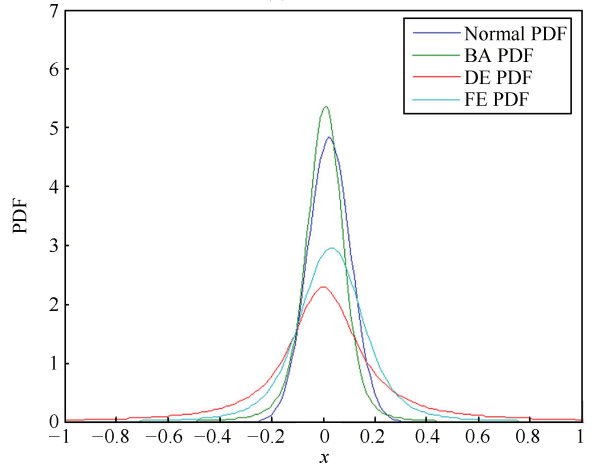

(c) Outer race PDF

Fig. 6. PDF of the bearing fault signals. (a) PDF of inner race fault signals in DE, FE and BA. (b) PDF of the ball fault signals in DE, FE and BA. (c) PDF of the outer race fault signals in DE, FE and BA.

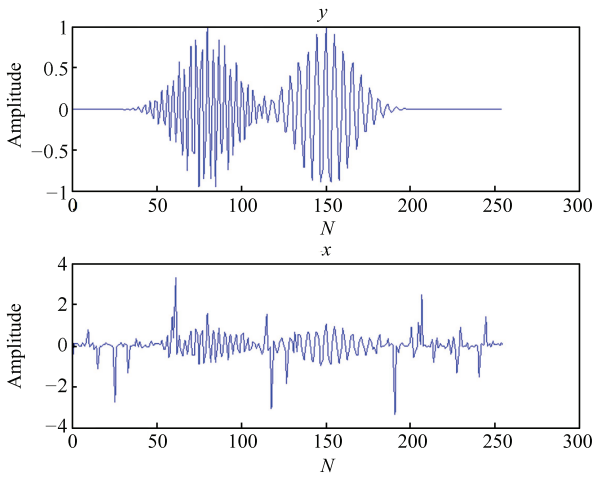

(a) Waveform of x and y

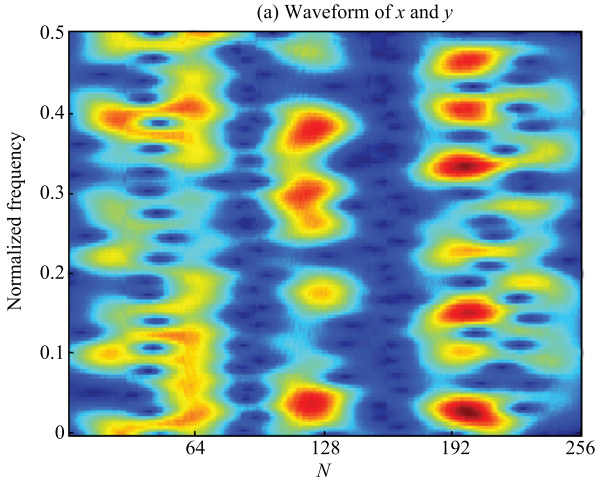

(b) STFT method

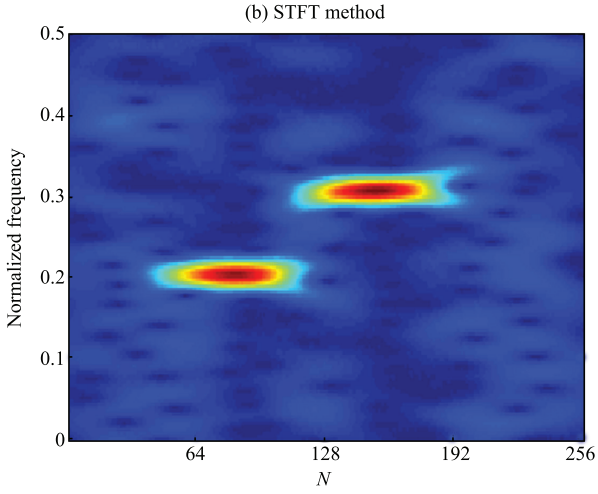

(c) FLO-STFT method

Fig. 7. Time-frequency representations of the signal x in $S\alpha S$ noise environment. (a) Waveform of x and y. (b) STFT time-frequency representation of the signal x. (c) FLO-STFT time-frequency representation of the signal x.

$$FLOSTFT_x(t,\omega) = \int_{-\infty}^{+\infty} x^{\langle P\rangle}(\tau)h(\tau - t)e^{-j\omega\tau}d\tau. \quad (16)$$

FLO-STFT discrete equation is defined as

$$FLOSTFT_x(n,\varpi) = \sum_{m} x^{\langle P\rangle}(m)h(m-n)e^{-jn\varpi}. \quad (17)$$

In (16) and (17), the moving window function can satisfy that P moment of non-stationary signal is stationary and integrable within the time window, however, the traditional STFT method is no longer stationary and integrable because $E[|s|] = \infty$ when $\alpha < 1$.

2) Application Review: We apply FLO-STFT time-frequency distribution to estimate the time-varying spectral, the signal x added with $S\alpha S$ distribution noise is defined as

$$x = e^{-a(n-80)^2+j\omega_1(n-80)} + e^{-a(n-190)^2+j\omega_2(n-190)} + S\alpha S = y + S\alpha S \quad (18)$$

where $a = 0.002$, $\omega_1 = 1.85$, $\omega_2 = 1.2$, $n = 1, 2, \ldots, 256$, $\alpha = 1.5$, $MSNR = 15$ dB (mixed signal to noise ratio), $MNSR = 10\log(E\{|s(t)|^2\}/\gamma^\alpha)$. The traditional STFT method and FLO-STFT method are used to estimate time-frequency representations of the signal x, simulation results are shown in Fig. 7.

3) Remarks: Fig. 7 (b) shows that the traditional STFT time-frequency method fails in noise environment, the improved FLOC-STFT method shows good robustness in Fig. 7 (c). However, the time-frequency resolution of the FLO-STFT method is controlled by the length of the window function like STFT method. In real application, the shorter time window should be used when we want to get the information of higher frequency components, and if we wish to closely localize the frequency location of lower frequency components, a longer time window is preferred. As a result, STFT time-frequency method is only suitable to analyze signals in Gaussian environment, but FLO-STFT can work in Gaussian and noise environment, which is robust.

B. Fractional Lower Order Wigner-Ville Distributions

1) Principle: Wigner-Ville distribution (WVD) of the signal $x(t)$ is defined as

$$WVD_x(t,\omega) = \int_{-\infty}^{+\infty} x\left(t+\frac{\tau}{2}\right) x\left(t-\frac{\tau}{2}\right) e^{-j\omega\tau} d\tau. \quad (19)$$

WVD time-frequency is a quadratic transformation, it has serious cross-terms, hence, the smoothing window function $h(\tau)$ is used to reduce the cross-term interference, Pseudo WVD (PWVD) is expressed as

$$PWVD_x(t,\omega) = \int_{-\infty}^{+\infty} h(\tau) x\left(t+\frac{\tau}{2}\right) x\left(t-\frac{\tau}{2}\right) e^{-j\omega\tau} d\tau. \quad (20)$$

In α stable distribution environment, fractional low order Wigner-Ville distribution (FLO-WVD) based on P order moment can be expressed as

$$FLOWVD_x(t,\omega) = \int_{-\infty}^{+\infty} x^{\langle P\rangle}\left(t+\frac{\tau}{2}\right) x^{-\langle P\rangle}\left(t-\frac{\tau}{2}\right) e^{-j\omega\tau} d\tau. \quad (21)$$

The FLO-WVD discrete equation of the signal $x(t)$ is expressed as

$$FLOWVD_x(n,\varpi) = 2\sum_m x^{\langle P\rangle}(n+m) x^{-\langle P\rangle}(n-m) e^{-jm\varpi}. \quad (22)$$

FLO-PWVD of the signal $x(t)$ can be defined as

$$FLOPWVD_x(t,\omega) = \int_{-\infty}^{+\infty} h(\tau) x^{\langle P\rangle}\left(t+\frac{\tau}{2}\right) x^{-\langle P\rangle}\left(t-\frac{\tau}{2}\right) e^{-j\omega\tau} d\tau. \quad (23)$$

The instantaneous auto-covariance of the signal $x(t)$ is defined as

$$R_x^C(t,\tau) = x^{\langle P\rangle}\left(t+\frac{\tau}{2}\right) x^{-\langle P\rangle}\left(t-\frac{\tau}{2}\right). \quad (24)$$

According to (24), FLO-WVD changes as

$$FLOWVD_x(t,\omega) = \int_{-\infty}^{+\infty} R_x^C(t,\tau) e^{-j\omega\tau} d\tau. \quad (25)$$

According to (24), we can know that FLO-WVD of the signal $x(t)$ is the Fourier transform of instantaneous auto-covariance in time delay τ.

2) Application Review: The traditional WVD method, PWVD method, the improved FLO-WVD method and FLO-PWVD method are used to estimate time-frequency distributions of the signal $x(t)$, and their simulation results are shown in Fig. 8.

3) Remarks: Fig. 8 (a) and Fig. 8 (c) respectively are WVD and PWVD time-frequency representations of the synthetic signal x, Fig. 8 (b) and Fig. 8 (d) respectively are FLO-WVD and FLO-PWVD of the synthetic signal x. Simulation results show WVD and PWVD time-frequency methods cannot work, but FLO-WVD and FLO-PWVD time-frequency methods have good performance in $S\alpha S$ environment. FLO-WVD method is an improved WVD time-frequency method, FLO-WVD has high time-frequency resolution, but it has serious cross-term interference. Hence, its application is inevitably hindered by the cross-term interference. FLO-PWVD is FLO-WVD added the window function, it can better suppress the cross term interference.

C. Fractional Lower Order Cohen Class Time-frequency Distributions

1) Principle: The Cohen-class time-frequency distribution is intended to obtain the expected properties like higher resolution, non-negativeness and removal of cross-terms with a kernel function, Cohen class time-frequency distribution (CTFD) of the analytic signal $x(t)$ is defined as

$$C_x(t,\omega) = \frac{1}{2\pi}\int_{-\infty}^{+\infty}\int_{-\infty}^{+\infty}\int_{-\infty}^{+\infty} x\left(t+\frac{\tau}{2}\right) x\left(t-\frac{\tau}{2}\right) \times \Phi(\theta,\tau) e^{j\theta t - j\omega\tau - j\theta u} d\theta d\tau du. \quad (26)$$

Ambiguity function (AF) of the signal $x(t)$ is expressed as

$$AF_x(\theta,\tau) = \int_{-\infty}^{+\infty} x\left(t+\frac{\tau}{2}\right) x\left(t-\frac{\tau}{2}\right) e^{-j\theta t} dt = \int_{-\infty}^{+\infty} R_x^C(t,\tau) e^{-j\theta t} dt. \quad (27)$$

Fractional low order ambiguity function (FLOAF) of the analytic signal $x(t)$ based on P order moment is defined as

$$FLOAF_x(\theta,\tau) = \int_{-\infty}^{+\infty} R_x^C(t,\tau) e^{-j\theta t} \mathrm{d}t = \int_{-\infty}^{+\infty} x^{\langle P\rangle}\left(t+\frac{\tau}{2}\right) x^{-\langle P\rangle}\left(t-\frac{\tau}{2}\right) e^{-j\theta t} dt. \quad (28)$$

When the inverse Fourier transform of (28) is computed, we can get:

$$R_x^C(t,\tau) = \frac{1}{2\pi}\int_{-\infty}^{+\infty} FLOAF_x(\theta,\tau) e^{j\theta t} d\theta. \quad (29)$$

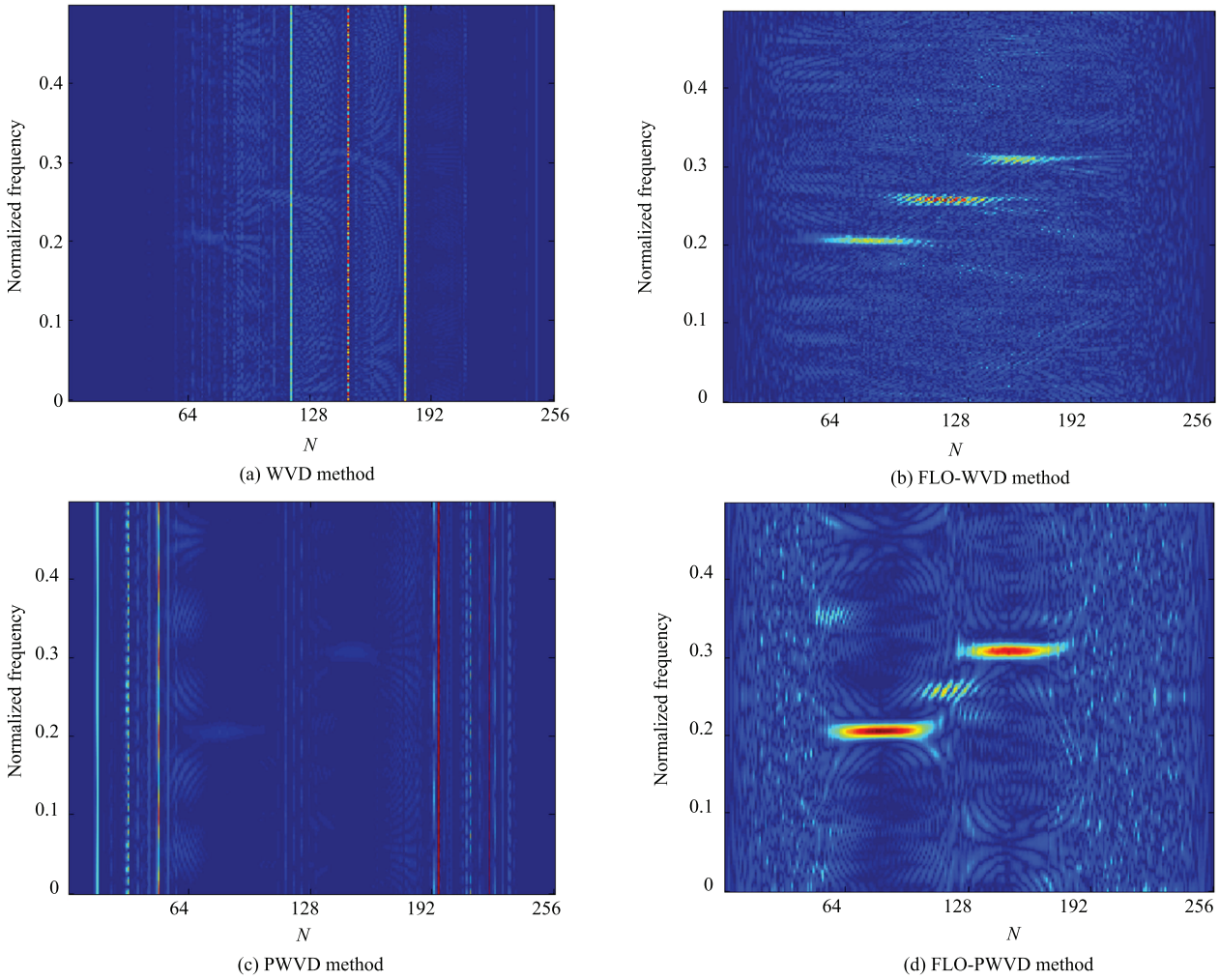

Fig. 8. Time-frequency representations of the signal x in $S\alpha S$ noise environment. (a) WVD time-frequency representation of the signal x. (b) FLO-WVD time-frequency representation of the signal x. (c) PWVD time-frequency representation of the signal x. (d) FLO-PWVD time-frequency representation of the signal x.

If (29) is substituted to (25), we get the following form:

$$FLOWVD_x(t,\omega) = \frac{1}{2\pi}\int_{-\infty}^{+\infty}\int_{-\infty}^{+\infty} FLOAF_x(\theta,\tau)e^{j\theta t - j\omega\tau}d\theta d\tau. \quad (30)$$

From (30), we know that FLOWVD of the signal $x(t)$ is two-dimensional Fourier transform of FLOC-AF, FLOWVD is three-dimensional (3-D) indication of the signal $x(t)$ in time, frequency and energy, and FLOC-AF is 3-D indication in time-delay, frequency deviation and the correlation. The images of FLOWVD and FLOC-AF have the components and cross-terms, the components of FLOWVD method are on both sides, and the cross terms are in the middle. However, the components of FLOC-AF are in the middle, and the cross terms are in both sides. When FLOC-AF of the signal $x(t)$ is computed, and a low-pass filter is used to filter cross-terms in AF plane, finally, the time-frequency distribution is calculated. FLO-Cohen distribution of the signal $x(t)$ is defined as

$$FLO-C_x(t,\omega) = \frac{1}{2\pi}\int_{-\infty}^{+\infty}\int_{-\infty}^{+\infty}\Phi(\theta,\tau) \times FLOAF_x(\theta,\tau)e^{j\theta t - j\omega\tau}d\theta d\tau. \quad (31)$$

$\Phi(\theta,\tau)$ is the kernel function, a different distribution is got when a different kernel function is used. If $\Phi(\theta,\tau) = 1$, FLO-Cohen time-frequency representation degenerates into FLOWVD method, when $\Phi(\theta,\tau)$ is a moving window function, FLO-Cohen method is called pseudo FLOWVD time-frequency representation, if $\Phi(\theta,\tau) = \cos(\theta\tau/2)$, FLO-Cohen method is called FLO- Rihaczek time-frequency representation, when $\Phi(\theta,\tau) = e^{j\theta\tau/2}$, FLO-Cohen method is called FLO-Page time-frequency representation, if $\Phi(\theta,\tau) = e^{-\theta^2\tau^2/\sigma}$, FLO-Cohen method is called FLO-Choi-Williams time-frequency representation, $\sigma$is a constant between $0.2-8$, if $\Phi(\theta,\tau) = g(\tau)\,|\tau|\,\sin(\beta\theta\tau)/\beta\theta\tau$, it is called as FLO-conical kernel distribution.

2) Application Review: Choi-Williams and FLO-Choi-Williams time-frequency methods are used to estimate time-frequency distributions of the synthetic signal x (18), simulation results are shown in Fig. 9.

3) Remarks: Fig. 9 (a) shows the Choi-Williams time-frequency representation of the synthetic signal x, and Fig. 9 (b) is the FLO-Choi-Williams time-frequency representation of the synthetic signal x. In view of the $S\alpha S$ stable distribution noise environment, the Choi-Williams method fails,

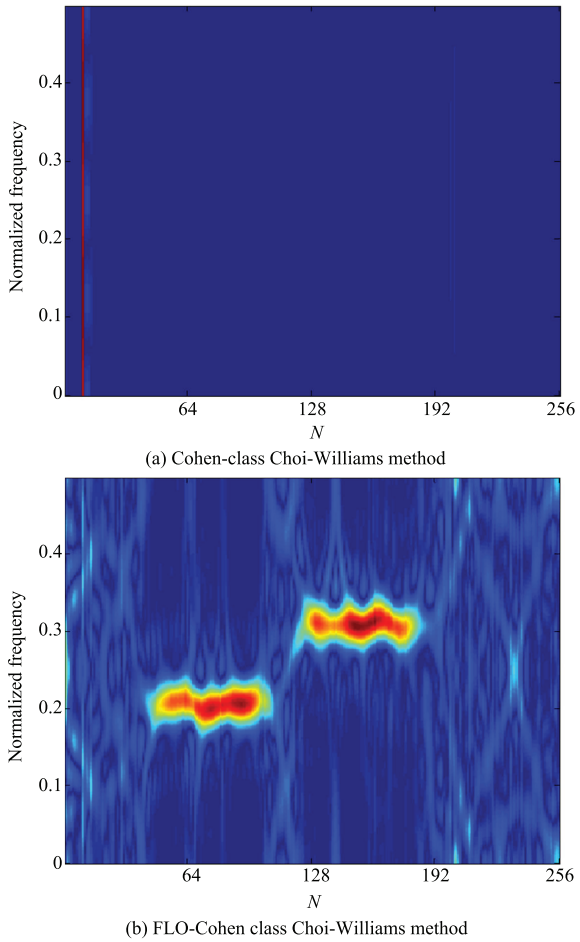

(a) Cohen-class Choi-Williams method

(b) FLO-Cohen class Choi-Williams method

Fig. 9. Time-frequency representations of the signal x in $S\alpha S$ noise environment. (a) Choi-Williams time-frequency representation of the signal x. (b) FLO-Choi-Williams time-frequency representation of the signal x.

and FLO-Choi-Williams method can better represent time-frequency distribution. FLO-Choi-Williams time-frequency method smoothing by the kernel function get rid of most of the cross-terms, but the time-frequency resolution is reduced.

D. FLO Adaptive Kernel Time-frequency Representation Method

1) Principle: The kernel functions of traditional Cohen-class time-frequency method and fractional lower order Cohen-class time-frequency method are fixed, a class kernel function is only suitable for one type of signal, which can not meet all the signals. However, the adaptive kernel time-frequency distribution can change optimal kernel function $\Phi(\theta,\tau)$ according to the feature of the different signals. Hence, adaptive optimal kernel time-frequency method is focused, and adaptive optimal kernel time-frequency representation in stable distribution environment will be a new direction.

According to the definition of FLOC-Cohen method, we use the optimal kernel function $\Phi_{\rm opt}(\theta,\tau)$ instead of the fixed kernel function $\Phi(\theta,\tau)$, then we can get a new fractional low-order adaptive kernel time-frequency distribution. the polar coordinates expression of optimal kernel can be defined as

$$\max_{\Phi}\int_0^{2\pi}\int_0^{+\infty}|AF_x(r,\phi)\Phi(r,\phi)|^2 r dr d\phi. \tag{32}$$

When the kernel function is a radial Gaussian kernel function, the optimal kernel function is defined as

$$\Phi(r,\phi)=e^{-\frac{r^2}{2\sigma^2(\phi)}} \tag{33}$$

where ϕ is radial angle, $\phi=\arctan(\tau/\theta)$, $\sigma(\phi)$ is radial extension functionit controls the radial shape of $\Phi(\theta,\tau)$, constraint condition in polar coordinates is defined as

$$\begin{aligned}&\frac{1}{4\pi^2}\int_0^{2\pi}\int_0^{+\infty}|\Phi(r,\phi)|^2 r dr d\phi\\&=\frac{1}{4\pi^2}\int_0^{2\pi}\int_0^{+\infty}\left|e^{-\frac{r^2}{2\sigma^2(\phi)}}\right|^2 r dr d\phi\\&=\frac{1}{4\pi^2}\int_0^{2\pi}\sigma^2(\phi)d\phi\le\beta.\end{aligned} \tag{34}$$

When $\Phi_{\rm opt}(\theta,\tau)$ is a radial optimal parabolic kernel function, its function is defined as

$$\Phi(\theta,\tau)=1-\frac{w(\theta^2+\tau^2)}{2\sigma^2(\phi)},\quad 0\le\frac{w(\theta^2+\tau^2)}{2\sigma^2(\phi)}\le 1. \tag{35}$$

The constraint condition in polar coordinates is expressed as

$$\frac{1}{6w\pi}\int_0^{\pi}\sigma^2(\phi)d\phi\le\beta. \tag{36}$$

If we use (32)−(34) to choose kernel function, the method can be called fractional lower order adaptive Gaussian-kernel time-frequency distribution (FLO-AGK-TFD). When we use (32), (35) and (36) to choose kernel function, it is called fractional lower order adaptive parabolic kernel time-frequency distribution (FLO-APK-TFD).

2) Application Review: The adaptive kernel function time-frequency distribution and FLO-adaptive kernel function time-frequency distribution are used to estimate time-frequency distributions of the synthetic signal x (18), the optimal radial Gaussian kernel function is used in the methods. Simulation results are shown in Fig. 10.

3) Remarks: The adaptive kernel time-frequency distributions of synthetic signal x are illustrated in Fig. 10 (a), and Fig. 10 (b) illustrate the FLO-adaptive optimal kernel time-frequency distributions of synthetic signal x. As shown in the figures, two components of the FLO-adaptive optimal kernel time-frequency method can be clearly resolved in fine resolution, but adaptive optimal kernel time-frequency method cannot represent time-frequency distributions. From Fig. 10 (b), we know that the FLO-adaptive kernel function method can effectively suppress the cross-terms, and it has a better time-frequency resolution. The FLO-adaptive kernel method requires that the auto-terms of the signals concentrate around the origin on the ambiguity plane, the cross-terms distribute in an area is far from the origin, and it will not be effective to separate the auto-terms and cross-terms when they overlap regardless of what volume of parameter is used.

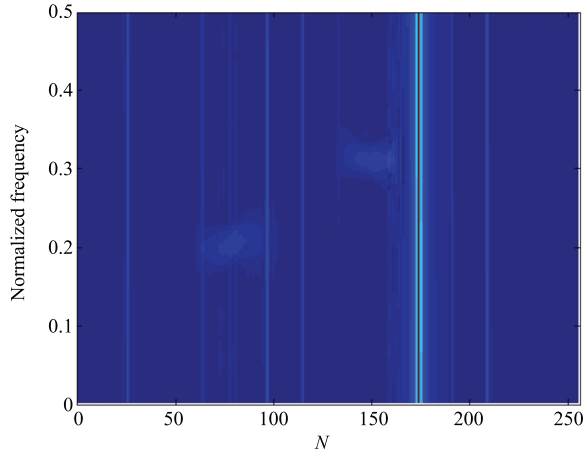

(a) Adaptive kernel time frequency representation

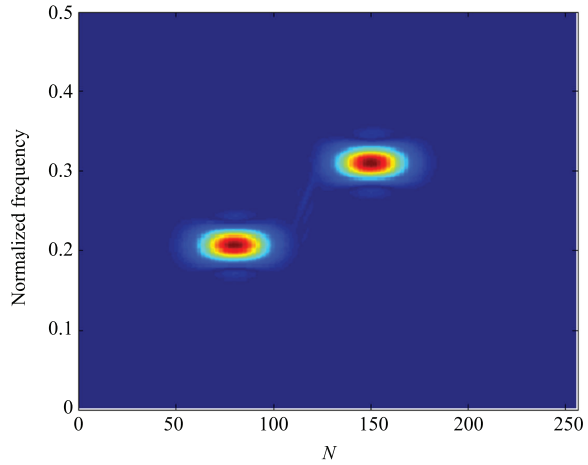

(b) FLO-adaptive kernel time frequency representation

Fig. 10. Time-frequency representations of the signal x in $S\alpha S$ noise environment. (a) Adaptive kernel time-frequency representation of the signal x. (b) FLO-adaptive kernel time-frequency representation of the signal.

E. Adaptive FLO-TFARMA Time-frequency Representation Method

TFARMA model of a non-stationary random process is defined as [19]

$$x[n] = -\sum_{i=1}^{M} a_i[n]x[n-i] + \sum_{i=0}^{L} b_i[n]e[n-i], \quad n = 0,1,2,\ldots,N-1 \tag{37}$$

where $a_i[n]$ and $b_i[n]$ are the time-varying parameters of the TFAR and TFMA part, M and L are orders, $e(n)$ is stationary white noise. When the noise $e(n)$ is a stationary $S\alpha S$ distribution process $u(n)$, according to the definition method of (37) TFARMA, we can also define a non-stationary time-frequency auto-regressive moving average $S\alpha S$ process TFARMA(M, L, A, B) as

$$x[n] = -\sum_{i=1}^{M} a_i[n]x[n-i] + \sum_{i=0}^{L} b_i[n]u[n-i], \quad n = 0,1,2,\ldots,N-1 \tag{38}$$

where

$$\begin{aligned} a_i[n] &= \sum_{l=-A}^{A} a_{i,l} f_l[n] \\ &= \sum_{l=-A}^{A} a_{i,l} e^{j\frac{2\pi}{N}nl}, \quad n = 0,1,2,\ldots,N-1 \\ b_i[n] &= \sum_{l=-B}^{B} b_{i,l} f_l[n] \\ &= \sum_{l=-B}^{B} b_{i,l} e^{j\frac{2\pi}{N}nl}, \quad n = 0,1,2,\ldots,N-1 \\ f_l[n] &= e^{j\frac{2\pi}{N}nl}, \quad l = 0,1,2,\ldots,\max\{A,B\}. \end{aligned} \tag{39}$$

We call it as fractional lower order time-frequency auto-regressive moving average (FLO-TFARMA) process, where M, L, A and B are the orders of the model, and M and L are the order in time domain, A and B are the order in frequency domain (the bandwidth of the model are $[-A, A]$ and $[-B, B]$), $a_i[n]$ and $b_i[n]$ are the parameters of the FLO-TFAR model, the numbers are as high as $N(M+L+1)$, $a_{i,l}$ and $b_{i,l}$ are basis expansion of the parameter functions, the number of $a_{i,l}$ is $M(2A+1)$, the number of $b_{i,l}$ is $(L+1)(2B+1)$. When $L = 0$, $B = 0$, FLO-TFARMA model will degrade into FLO-TFAR(M, A) model, and if $A = 0$, $B = 0$, it will degrade into FLO-TFMA(M, L) model. $f_l[n]$ is the basis functions, $u(n)$ is a stationary white noise $S\alpha S$ process, γ is its dispersion coefficient ($\gamma = 1$).

1) FLO-TFMA Time-frequency Representations: The α spectrum of the α stable distribution process is defined as [33]

$$\begin{aligned} S_\alpha(z) &= \left[X[n], \sum_{i=-q}^{q} X(n-i)z^i\right] \\ &= \gamma\left[\left(\frac{1}{z}\right)^{\langle\alpha-1\rangle}\right][H(z)]^{\langle\alpha-1\rangle}. \end{aligned} \tag{40}$$

When inserting $z = e^{j\omega}$ into (40), α spectrum on the unit circle is calculated as

$$S_\alpha(e^{j\omega}) = \gamma H(e^{j\omega})[H(e^{j\omega})]^{\langle\alpha-1\rangle} = \gamma\left|H(e^{j\omega})\right|^{\alpha}. \tag{41}$$

When Z transformation with respect to both sides of (38) is computed, we obtain

$$H[Z] = \frac{1+\sum_{i=1}^{L} b_i[n]Z^{-i}}{1+\sum_{i=1}^{M} a_i[n]Z^{-i}} = \frac{B(Z)}{A(Z)}. \tag{42}$$

By inserting (42) into (40), FLO-TFARMA model spectrum estimation of a $S\alpha S$ process $X[n]$ can be defined as

$$S_\alpha(n,k) = \gamma\left|\frac{1+\sum_{i=1}^{L} b_i[n]e^{-j\frac{2\pi}{N}ik}}{1+\sum_{i=1}^{M} a_i[n]e^{-j\frac{2\pi}{N}ik}}\right|^{\alpha}$$

$$= \gamma \left| \frac{1 + \sum_{i=1}^{L} \sum_{l=-B}^{B} b_{i,l} e^{-j\frac{2\pi}{N}(ik-nl)}}{1 + \sum_{i=1}^{M} \sum_{l=-A}^{A} a_{i,l} e^{-j\frac{2\pi}{N}(ik-nl)}} \right|^{\alpha}. \quad (43)$$

For getting $a_{i,l}$ and $b_{i,l}$ of FLO-TFARMA model parameters, we solve the parameters $a_{i,l}$ of FLO-TFAR model, and then solve the parameters $b_{i,l}$ of FLO-TFMA model.

2) FLO-TFAR Parameters Estimation: If both sides of (38) are multiplied by $x^{\langle P-1\rangle}[n-i']$ and taken expectation, it can be written as

$$\sum_{i'=0}^{M} a_i[n] E\left\{x[n-i']x^{\langle P-1\rangle}[n-i']\right\} = \sum_{i'=0}^{L} b_i[n] E\left\{U[n-i']x^{\langle P-1\rangle}[n-i']\right\}. \quad (44)$$

A simplified fractional lower order covariance is defined in [21], it simplifies to (44), and then we can get

$$\sum_{i'=0}^{M} \sum_{l'=-A}^{A} a_{i',l'} C_x[n-i', i-i'] e^{j\frac{2\pi}{N}nl'} = \sum_{i'=0}^{L} \sum_{l'=-B}^{B} b_{i',l'} C_{U,x}[n-i', i-i'] e^{j\frac{2\pi}{N}nl'} \quad (45)$$

where

$$C_x[n-i', i-i'] = E\left\{x[n-i']x^{\langle P-1\rangle}[n-i']\right\} = E\left\{x[n-i']|x[n-i']|^{P-2}X^*[n-i']\right\}$$

is auto-covariance function of $x[n]$, and

$$C_{U,x}[n-i', i-i'] = E\left\{U[n-i']x^{\langle P-1\rangle}[n-i']\right\} = E\left\{U[n-i']|x[n-i']|^{P-2}\cdot x^*[n-i']\right\}$$

is cross-covariance of $x[n]$ and $U[n]$, N points of discrete Fourier transform (DFT) with respect to both sides of (45) can be expressed as

$$\sum_{i'=0}^{M} \sum_{l'=-A}^{A} a_{i',l'} \lambda_x[i-i', l-l'] e^{-j\frac{2\pi}{N}i'(l-l')} = \sum_{i'=0}^{L} \sum_{l'=-B}^{B} b_{i',l'} \lambda_{U,x}[i-i', l-l'] e^{-j\frac{2\pi}{N}i'(l-l')} \quad (46)$$

$$\lambda_x[i-i', l-l'] = \sum_{n=0}^{N-1} C_x[n-i', i-i'] e^{-j\frac{2\pi}{N}nl'}$$

$$\lambda_{U,x}[i-i', l-l'] = \sum_{n=0}^{N-1} C_{U,x}[n-i', i-i'] e^{-j\frac{2\pi}{N}nl'} \quad (47)$$

where $\lambda_x[i-i', l-l']$ and $\lambda_{U,x}[i-i', l-l']$ are similar to Cohen-class time-frequency distribution expected ambiguity function (EAF) based on the second-order correlation function $A_x[i,l] = \sum_{n=0}^{N-1} R_X[n,i] e^{-j\frac{2\pi}{N}nl}$, its auto-correlation is replaced by auto-covariance, it can be named as fractional order discrete expect ambiguity function (FLO-EAF), it represents statistical covariance of the time shift and frequency shift in time-frequency domain. When $i \geq A$, $x[n]$, $U[n]$ are statistically independent from each other and $C_{U,x}[n-i', i-i'] = 0$, (46) can be written as

$$\sum_{i'=0}^{M} \sum_{l'=-A}^{A} a_{i',l'} \lambda_x[i-i', l-l'] e^{-j\frac{2\pi}{N}i'(l-l')} = 0$$

$$\sum_{i'=1}^{M} \sum_{l'=-A}^{A} a_{i',l'} \lambda_x[i-i', l-l'] e^{-j\frac{2\pi}{N}i'(l-l')} = -\lambda_x[i,l], \quad A+1 \leq i \leq A+M \ -L \leq l \leq L \quad (48)$$

Equation (48) can be written as

$$\Gamma a = -\theta \ \text{ or } a = -\Gamma^{-1}\theta \quad (49)$$

where Γ is $(2L+1)M \times (2L+1)M$ Toeplitz-block matrix, $a = [a_1^T, a_2^T, \ldots, a_M^T]^T$, $a_m = [a_{i,-L}, a_{i,-L+1}, \ldots, a_{i,L}]^T$, $\theta = [\theta_{A+1}^T, \theta_{A+2}^T, \ldots, \theta_{A+M}^T]^T$.

Equation (49) has $(2L+1)M$ independent equations, and the required parameters $a_{i',l'}$ are $(2L+1)M$. The lengths of θ and a are $(2L+1)M$, and through the solution of Toeplitz matrices using (49), we can obtain the vector a and FLO-TFAR model parameters $a_{i,l}$.

3) FLO-TFMA Parameters Estimation: A $S\alpha S$ distribution signal $y[n]$ can be produced by $S\alpha S$ noise distribution $U[n]$ through causal linear time-varying (LTV) system (TFMA), we can also obtain it when $U[n]$ is passed through a TFARMA system and then through a TFAR model system. Then, we can take advantage of the observation sequence $x[n]$ that is discussed in Section V-B with the help of TFAR model filter to obtain TFMA process $y[n]$, this whole process can be expressed as

$$y[n] = \sum_{i=0}^{L} b_i[n] U[n-i] = \sum_{i=0}^{L} \sum_{l=-B}^{B} b_{i,l}[n] e^{j\frac{2\pi}{N}nl} U[n-i]. \quad (50)$$

The both sides of (50) are multiplied by $x^{\langle P-1\rangle}[n-i']$ and taken expectation, then, N points of discrete Fourier transform (DFT) with respect to both sides of (50) can be written as

$$\sum_{i'=0}^{L} \sum_{l'=-B}^{B} b_{i',l'}[n] \lambda_{U,y}[i-i', l-l'] e^{-j\frac{2\pi}{N}i'(l-l')} = \lambda_y[i,l], \quad 0 \leq i \leq L, \ -B \leq i \leq B. \quad (51)$$

When $LB \ll N$, phase factor $e^{-j\frac{2\pi}{N}i'(l-l')} \approx 1$, it can be expressed as

$$\sum_{i'=0}^{L} \sum_{l'=-B}^{B} b_{i',l'}[n] \lambda_{U,y}[i-i', l-l'] = \lambda_y[i,l], \quad 0 \leq i \leq L, \ -B \leq i \leq B. \quad (52)$$

According to the method in Section V-B, (49) is written as Toeplitz matrix form $\Gamma b = \theta$, and then the model parameters $b_{i,l}$ are solved.

However, $U[n]$ and $\lambda_{U,y}[i-i', l-l']$ are unknown from the observations of a random signal $x[n]$, in that way, we cannot evaluate $b_{i,l}$ through the above method. We can use

improved fractional lower order complex time-frequency spectrum (FLO-CTFC) algorithm to calculate FLO-TFMA coefficient $b_{i,l}$ [34], where, the second order correlation is replaced by fractional low-order covariance.

4) Application Review: We will study the performances of the TFAR, TFMA and TFARMA, the proposed FLO-TFAR, FLO-TFMA and FLO-TFARMA, they are applied to estimate the time frequency representations of the synthetic signal x (18) in $S\alpha S$ stable distribution noise environment. The length of the signal $N = 256$, its time frequency representations are shown in Figs. 11−13.

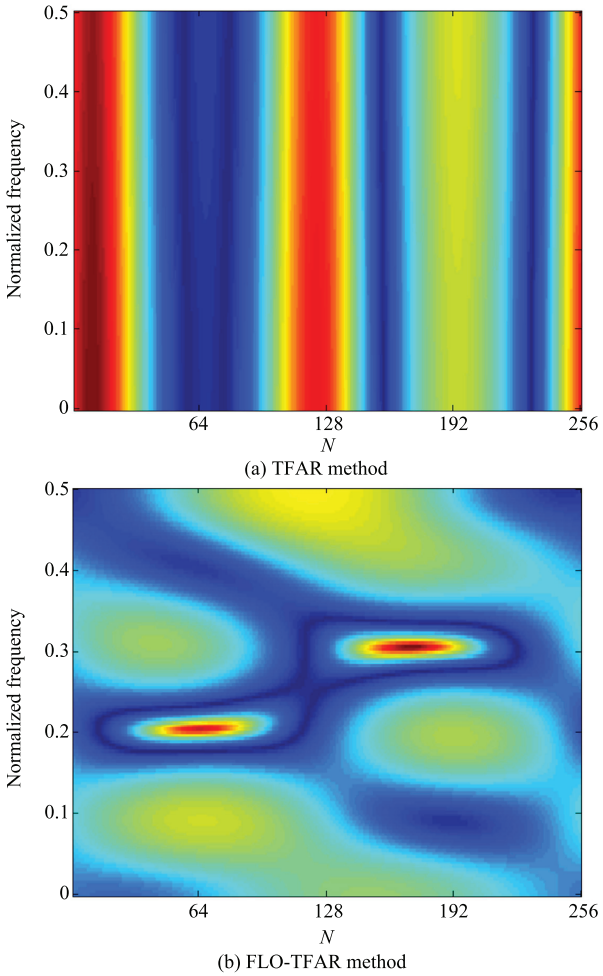

Fig. 11. The model time-frequency representations of the signal x in $S\alpha S$ noise environment. (a) TFAR(5, 1) model time-frequency representation of the signal x. (b) FLO-TFAR(5, 1) model time-frequency representation of the signal.

5) Remarks: The results show that TFAR(5, 1) model time-frequency spectrum is a failure in Fig. 11 (a), the overall resolution of FLO-TFAR(5, 1) is poorer than that of the nonparametric FLO-PWVD in Fig. 11 (b). but it can better suppress the cross term interference. TFMA(2, 2) method failed in Fig. 12 (a), and FLO-TFMA(2, 2) spectrum is very poor in Fig. 12 (b). Finally, TFARMA(2, 2, 1, 2) model method cannot work in $S\alpha S$ noise environment in Fig. 13 (a), but FLO-TFARMA(2, 2, 1, 2) model time-frequency spectrum exhibits better resolution than FLO-TFAR and FLO-TFMA in Fig. 13 (b), and it does not contain any cross terms as does FLO-PWVD.

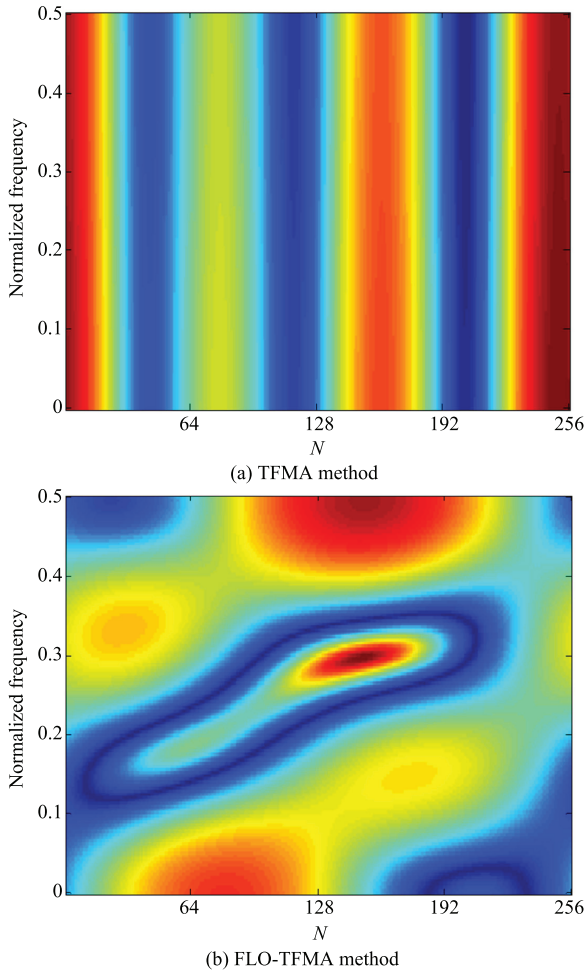

Fig. 12. The model time-frequency representations of the signal x in $S\alpha S$ noise environment. (a) TFMA(2, 2) model time-frequency representation of the signal x. (b) FLO-TFMA(2, 2) model time-frequency representation of the signal.

The improved FLO-TFAR, FLO-TFMA and FLO-TFARMA methods are effective for slowly time-varying signals, and they are free from cross-term interference. The time-frequency resolution of the FLO-TFAR and FLO-TFMA methods are relatively low, and FLO-TFARMA method illustrates better resolution. In addition, the complicated algorithm for estimating model parameters makes FLO-TFARMA method computationally demanding. Therefore, some works will be made to improve the time-frequency resolution and model parameter estimation process for practical fault signal analysis.

V. Application Simulations

The impulse of the outer race fault signals in the vibration position of the drive end accelerometer, the fan end accelerom-

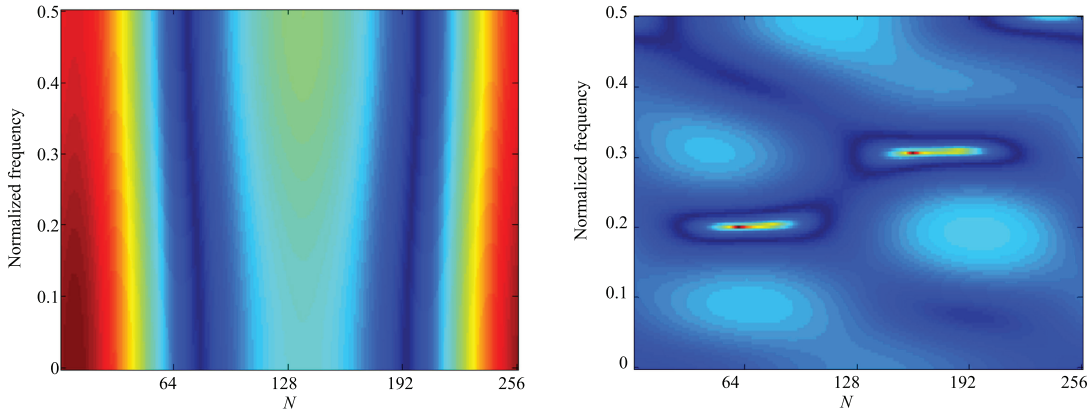

(a) TFARMA method (b) FLO-TFARMA method

Fig. 13. The model time-frequency representations of the signal x in $S\alpha S$ noise environment. (a) TFARMA$(2, 2, 1, 2)$ model time-frequency representation of the signal x. (b) FLO-TFARMA$(2, 2, 1, 2)$ model time-frequency representation of the signal.

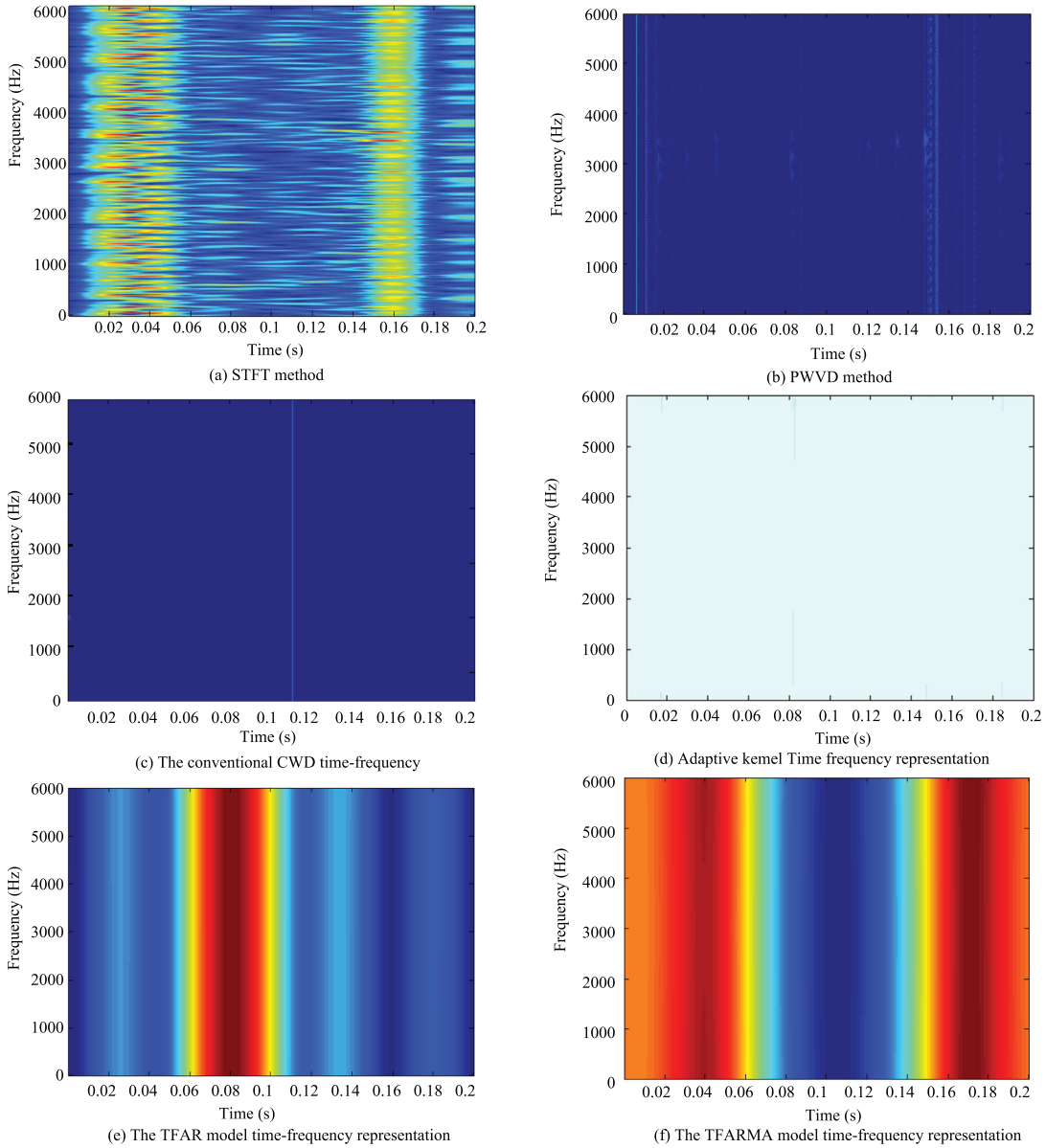

(a) STFT method (b) PWVD method

(c) The conventional CWD time-frequency (d) Adaptive kemel Time frequency representation

(e) The TFAR model time-frequency representation (f) The TFARMA model time-frequency representation

Fig. 14. The conventional time-frequency representations of the outer race fault signal in α stable distribution environment. (a) The conventional STFT time-frequency representation. (b) The conventional PWVD time-frequency representation. (c) The conventional CWD time-frequency representation. (d) The conventional adaptive kernel time-frequency representation. (e) The TFAR model time-frequency representation. (f) The TFARMA model time-frequency representation.

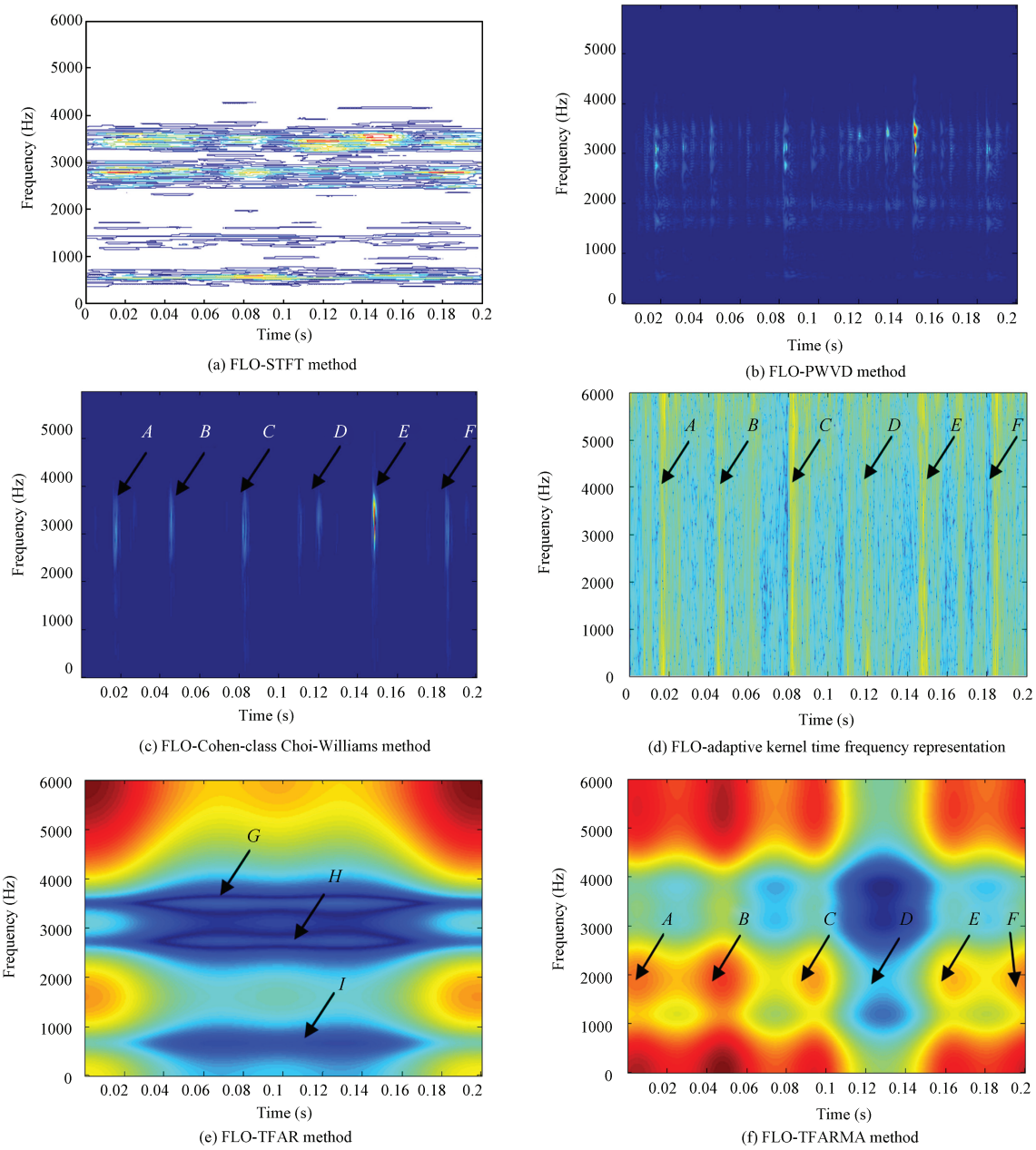

Fig. 15. The new time-frequency representations of the outer race fault signal in α stable distribution environment. (a) The FLO-STFT time-frequency representation. (b) The FLO-PWVD time-frequency representation. (c) The FLO-CWD time-frequency representation. (d) The FLO-adaptive kernel time-frequency representation. (e) The FLO-TFAR model time-frequency representation. (f) The FLO-TFARMA model time-frequency representation.

eter and the base accelerometer is generated because of the local defects of rolling element bearings, as shown Fig. 5 (d) and Table I. The fault signals are non-Gaussian and non-stationary α stable distribution because of the presence of impulses. α stable distribution noises are added to the fault signals in the experiment, setting $\alpha = 0.8$, $MSNR = 20$ dB, and letting $N = 2400$. The conventional time-frequency distribution methods including STFT, PWVD, CWD, the adaptive kernel time-frequency method, TFMA, TFARMA model time-frequency method, and the improved lower order time-frequency distribution methods including FLO-STFT, FLO-PWVD, FLO-CWD, the FLO-adaptive kernel time-frequency method, FLO-TFMA and FLO-TFARMA model time-frequency method are applied to analyze the vibration signal of a bearing with an artificially seeded defect on outer race in the position of DE in α stable distribution environment. FLO-TFMA(2, 2) and FLO-TFARMA(2, 2, 1, 2) model time-frequency spectrum methods are used to analyze the signals in the experiment. The results are shown in Figs. 14 and 15.

VI. CONCLUSIONS

STFT time-frequency representation of the outer race fault signal is shown in Fig. 14 (a). Fig. 14 (b) is the PWVD time-

TABLE II
THE COMPARISON OF VARIOUS FLO-TIME-FREQUENCY DISTRIBUTION METHODS

Methods	Advantages	Disadvantages	Application to fault diagnosis
FLO-STFT time-frequency distribution	Free from cross-terms, Low computational complexity, Definite physical meaning	Low time-frequency resolution	Revealing the time-frequency structure of the fault signals as a preprocessing tool
FLO-WVD time-frequency distribution	High time-frequency resolution	Serious cross-terms interference	Analyzing the fault signals after getting the signals structure
FLO-Cohen class time-frequency distribution	Suppressed cross-terms compared with FLO-WVD method	Reduced time-frequency resolution, certain cross-term interference	Analyzing the fault signals after getting the signals structure
FLO-adaptive kernel time-frequency distribution	Suppressed cross-terms, improved timeCfrequency resolution	High computationally complex	Suitable to the computational complexity fault signals
FLO-ARMA time-frequency distribution	Free from cross-terms	High computational complexity, low time-frequency resolution	Suitable to analyzing the slowly time-varying fault signals

frequency distribution, CWD method time-frequency representation is shown in Fig. 14 (c), the adaptive kernel time-frequency representation is in Figs. 15 (d)−15 (f), respectively, are TFAR model time-frequency representation and TFARMA model time-frequency distribution. The results show that the conventional time-frequency methods fail in α stable distribution environment. FLO-STFT time-frequency representations of the outer race fault signal in Fig. 15 (a) show the shock pulse is mainly distributed in low-frequency band from 0 Hz to 4000 Hz, and the transient harmonic vibration components of about 600 Hz, 2800 Hz and 3500 Hz dominate frequency-domain. Its vertical resolution is bad, the fault characteristic frequency cannot be seen. FLO-PWVD time-frequency representations in Fig. 15 (b) have a good vertical resolution, but there are serious cross terms, which render it not conducive to observe. FLO-CWD method preferably restrains the cross-term interference in Fig. 15 (c), it can be seen clearly that the gap regularly changes between the impact, the interval between the impulses A, B, C, D, E and F is approximately 30 ms, the interval corresponds to the characteristic frequency of outer race as 33.333 Hz. We can also know the interval between A, B, C, D, E and F is about 30 ms from FLO-adaptive kernel time-frequency representation in Fig. 15 (d), the impact frequency band expanded into 0−6000 Hz because of its poor lateral resolution. The results show that the transient harmonic vibration components are 600 Hz, 2800 Hz and 3500 Hz from the FLO-TFAR model time-frequency representation in Fig. 15 (e), but its vertical resolution is bad, so we cannot see the effect of the time interval. However, FLO-TFARMA model time-frequency distributions in Fig. 15 (f) show the interval between the impulses A, B, C, D, E and F is approximately 30 ms, as well as that the dominant frequency of 600 Hz, 2800 Hz and 3500 Hz, FLO-TFARMA has certain ability in the horizontal and vertical, but the overall resolution is low.

The simulations show that the improved methods have their respective advantages and disadvantages as shown in this paper. The fractional lower order short time Fourier transform time-frequency representation has low computational complexity and definite physical meaning, but the time-frequency resolution is low, hence it is suitable to analyze the non-stationary machinery fault signals whose local stationary is larger. The fractional lower Wigner-Ville time-frequency representation has high time-frequency resolution, however, there are serious cross-terms interference. The fractional lower order pseudo Wigner-Ville time-frequency representation added window function and the different kernel function fractional low-order Cohen class time-frequency distribution can suppress certain cross-term interference, but it leads to reduced the time-frequency resolution. The fractional lower order adaptive kernel time-frequency representation can suppress cross-term interference, and effectively improve the time-frequency resolution, but the computational complexity is higher. The fractional lower order ARMA model time-frequency representation has no interference of cross-terms, but the time-frequency resolution is low, hence it is suitable for analyzing the changing slowly non-stationary machinery fault signals. The methods are summarized in Table II. In real applications, several methods can be selected to analyze the fault signals according to their specific characteristics.

The paper has presented an accurate statistical parameter model $S\alpha S$ distribution for bearing fault signals diagnosis. The time-frequency analysis methods are key tools for machinery fault diagnosis, they can be used to identify the constituent components and time variation of the signals. We have presented FLO-STFT, FLO-WVD, FLO-PWVD, FLO-CWD, FLO-AKTFD and FLO-ARMA time-frequency analysis methods based on $S\alpha S$ stable distribution statistical model. The methods have better performances than the conventional methods including STFT, WVD, PWVD, CWD, AKTFD and ARMATFD. The traditional methods fail in $S\alpha S$ stable distribution environment, but the proposed methods can regularly work in the noise environment, which shows robustness. The proposed time-frequency analysis methods are used to analyze the bearing fault signals, they have respective advantages and disadvantages, the FLO-STFT method has low computational complexity and low resolution. FLO-WVD has better resolution, but there are serious cross terms. The FLO-PWVD and FLO-CWD methods suppress the cross-term interference through adding the window function, but they still suffer from

cross-term interference. The FLO-AKTFD methods could be effective to improve time-frequency resolution and suppress cross-terms. The FLO-TFARMA model method is free from cross-term interference, however, the time-frequency resolution is not as high as expected. The improved time-frequency analysis method is applied to the bearing fault diagnosis, which can better get fault features of the signals. In the actual bearing fault diagnosis analysis, we can use the above several kinds of comprehensive methods to analyze together, and take their respective advantages to comprehensive judgment, and hence better results can be obtained.

REFERENCES

[1] S. V. Narasimhan and S. Pavanalatha, "Estimation of evolutionary spectrum based on short time Fourier transform and modified group delay," *Signal Process.*, vol. 84, no. 11, pp. 2139−2152, Nov. 2004.

[2] B. P. Tang, W. Y. Liu, and T. Song, "Wind turbine fault diagnosis based on Morlet wavelet transformation and Wigner-Ville distribution," *Renew. Energy*, vol. 35, no. 12, pp. 2862−2866, Dec. 2010.

[3] Z. K. Peng, P. W. Tse, and F. L. Chu, "A comparison study of improved Hilbert-Huang transform and wavelet transform: Application to fault diagnosis for rolling bearing," *Mechan. Syst. Signal Process.*, vol. 19, no. 5, pp. 974−988, Sep. 2005.

[4] Z. P. Feng, M. Liang, and F. L. Chu, "Recent advances in timeCfrequency analysis methods for machinery fault diagnosis: A review with application examples," *Mechan. Syst. Signal Process.*, vol. 38, no. 1, pp. 165−205, Jul. 2013.

[5] J. H. Wang, L. Y. Qiao, Y. Q. Ye, and Y. Q. Chen, "Fractional Hilbert transform in rolling element bearings diagnostics," in *Proc. the 2015 Int. Symp. Fractional Signals and Systems*, Romania, 2015, pp. 1−3.

[6] M. A. Al-Manie and W. J. Wang, "Time-frequency analysis by evolutionary periodogram with application in gear fault diagnosis," *Int. J. Wavelets, Multiresolut. Inf. Process.*, vol. 8, no. 5, pp. 679−693, Apr. 2010.

[7] G. M. Dong and J. Chen, "Noise resistant time frequency analysis and application in fault diagnosis of rolling element bearings," *Mechan. Syst. Signal Process.*, vol. 33, pp. 212−236, Nov. 2012.

[8] R. G. Baraniuk and D. L. Jones, "Signal-dependent time-frequency analysis using a radially Gaussian kernel," *Signal Process.*, vol. 32, no. 3, pp. 263−284, Jun. 1993.

[9] R. G. Baraniuk and D. L. Jones, "A signal-dependent time-frequency representation: optimal kernel design," *IEEE Trans. Signal Process.*, vol. 41, no. 4, pp. 1589−1602, Apr. 1993.

[10] R. N. Czerwinski and D. L. Jones, "Adaptive cone-kernel time-frequency analysis," *IEEE Trans. Signal Process.*, vol. 43, no. 7, pp. 1715−1719, Jul. 1995.

[11] D. S. Wu and J. M. Morris, "Time-frequency representations using a radial Butterworth kernel," in *Proc. the IEEE-SP Int. Symp. Time-Frequency and Time-Scale Analysis*, Philadelphia, PA, USA, 1994, pp. 60−63.

[12] S. C. Wang, J. Han, J. F. Li, and Z. N. Li, "Adaptive signal analysis based on radial parabola kernel," *Appl. Mechan. Mater.*, vol. 10−12, pp. 737−741, Jan. 2008.

[13] H. Li, X. F. Liu, and L. Bo, "Chirplet time-frequency spectrum analysis of gear and rolling bearing fault," *J. Vib. Meas. Diagno.*, vol. 31, no. 5, pp. 591−595, Oct. 2011.

[14] S. C. Wang, J. Han, Z. N. Li, and J. F. Li, "Adaptive radial parabola kernel representation and its application in the fault diagnosis," *J. Mechan. Strength*, vol. 29, no. 2, pp. 180−184, Nov. 2007.

[15] D. F. Shi, F. Shen, M. Bao, and L. S. Qu, "Adaptive time-frequency analysis and its application in large rotating machinery diagnosis," *J. Vib. Eng.*, vol. 13, no. 2, pp. 271−276, Jun. 2000.

[16] M. Jachan, G. Matz, and F. Hlawatsch, "Time-frequency-autoregressive random processes: Modeling and fast parameter estimation," in *Proc. the 2003 IEEE Int. Conf. Acoustics, Speech, and Signal Processing*, Hong Kong, China, 2003.

[17] M. Jachan, G. Matz, and F. Hlawatsch, "Least-squares and maximum-likelihood TFAR parameter estimation for nonstationary processes," in *Proc. 2006 IEEE Int. Conf. Acoustics, Speech and Signal Processing*, Toulouse, France, 2006.

[18] M. Jachan, G. Matz, and F. Hlawatsch, "Vector time-frequency AR models for nonstationary multivariate random processes," *IEEE Trans. Signal Process.*, vol. 57, no. 12, pp. 4646−4658, Dec. 2009.

[19] M. Jachan, G. Matz, and F. Hlawatsch, "Time-frequency ARMA models and parameter estimators for underspread nonstationary random processes," *IEEE Trans. Signal Process.*, vol. 55, no. 9, pp. 4366−4380, Sep. 2007.

[20] L. R. Padovese, "Hybrid timeCfrequency methods for non-stationary mechanical signal analysis," *Mechan. Syst. Signal Process.*, vol. 18, no. 5, pp. 1047−1064, Sep. 2004.

[21] A. G. Poulimenos and S. D. Fassois, "Parametric time-domain methods for non-stationary random vibration modelling and analysisła critical survey and comparison," *Mechan. Syst. Signal Process.*, vol. 20, no. 4, pp. 763−816, May 2006.

[22] M. Shao and C. L. Nikias, "Signal processing with fractional lower order moments: Stable processes and their applications," *Proc. the IEEE*, vol. 81, no. 7, pp. 986−1010, Jul. 1993.

[23] X. Y. Ma and C. L. Nikias, "Parameter estimation and blind channel identification in impulsive signal environments," *IEEE Trans. Signal Process.*, vol. 43, no. 12, pp. 2884−2897, Dec. 1995.

[24] T. H. Liu and J. M. Mendel, "A subspace-based direction finding algorithm using fractional lower order statistics," *IEEE Trans. Signal Process.*, vol. 49, no. 8, pp. 1605−1613, Aug. 2001.

[25] X. Y. Ma and C. L. Nikias, "Joint estimation of time delay and frequency delay in impulsive noise using fractional lower order statistics," *IEEE Trans. Signal Process.*, vol. 44, no. 11, pp. 2669−2687, Nov. 1996.

[26] C. N. Li and G. Yu, "A new statistical model for rolling element bearing fault signals based on Alpha-stable distribution," in *Proc. the 2nd Int. Conf. Computer Modeling and Simulation*, Sanya, Hainan, China, 2010, pp. 386−390.

[27] X. M. Yu and T. Shu, "Fault diagnosis method for gearbox based on α-stable distribution parameters and support vector machines," *Meas. Control Technol.*, vol. 31, no. 8, pp. 23−26, 30, Aug. 2012.

[28] G. Yu, C. N. Li, and J. F. Zhang, "A new statistical modeling and detection method for rolling element bearing faults based on alphaC-stable distribution," *Mechan. Syst. Signal Process.*, vol. 41, no. 1−2, pp. 155−175, Dec. 2013.

[29] J. H. Wang, Y. Q. Ye, X. Pan, X. D. Gao, and C. Zhuang, "Fractional zero-phase filtering based on the RiemannCLiouville integral," *Signal Process.*, vol. 98, pp. 150−157, May 2014.

[30] J. H. Wang, Y. Q. Ye, Y. B. Gao, S. Q. Qian, and X. D. Gao, "Fractional

compound integral with application to ECG signal denoising," *Circuits Syst. Signal Process.*, vol. 34, no. 6, pp. 1915−1930, Jun. 2015.

[31] J. H. Wang, Y. Q. Ye, X. Pan, and X. D. Gao, "Parallel-type fractional zero-phase filtering for ECG signal denoising," *Biomed. Signal Process. Control*, vol. 18, pp. 36−41, Apr. 2015.

[32] CWRU, CWRU bearing data center, Accessed on: Sep. 25, 2015. [Online]. Available: http://csegroups.case.edu/bearingdatacenter/

[33] S. Y. Wang and X. B. Zhu, "α spectrum estimation method for ARMA α process based on FLOC," *J. Commun.*, vol. 28, no. 7, pp. 98−103, Jul. 2007.

[34] M. Jachan, G. Matz, and F. Hlawatsch, "Time-frequency-moving-average processes: Principles and cepstral methods for parameter estimation," in *Proc. IEEE Int. Conf. Acoustics, Speech, and Signal Processing*, Montreal, Que., Canada, 2004.

Junbo Long graduated from Hunan Normal University, China, in 2003. He received the M.Sc. degree from Dalian University of Technology, China, in 2013. He is currently a Lecturer at Jiujiang University. His research interests include fractional lower order signal processing and time-frequency signal processing.

Haibin Wang graduated from Hunan Normal University, China, in 2003. She received the M.Sc. degree from Huazhong University of Science and Technology, China, in 2010. She is currently a Lecturer at Jiujiang University. Her research interests include fractional lower order signal processing and image signal processing.

Peng Li graduated from Central China Normal University, China, in 2003. She received the M.Sc. degree from Huazhong University of Science and Technology, China, in 2008. She is currently a Lecturer at Jiujiang University. Her research interests include non-Gaussian signal processing and time-frequency signal processing.

Hongshe Fan graduated from Shaanxi University of Technology, China, in 1998. He received the M.Sc. degree from Radar University, China, in 2004. He is currently a Professor at Jiujiang University. His research interests include radar signal processing and communication signal processing.